

Defects in beta cell Ca^{2+} signalling, glucose metabolism and insulin secretion in a murine model of K_{ATP} channel-induced neonatal diabetes mellitus

R. K. P. Benninger · M. S. Remedi · W. S. Head ·
A. Ustione · D. W. Piston · C. G. Nichols

Received: 28 September 2010 / Accepted: 3 December 2010 / Published online: 27 January 2011
© Springer-Verlag 2011

Abstract

Aims/hypothesis Mutations that render ATP-sensitive potassium (K_{ATP}) channels insensitive to ATP inhibition cause neonatal diabetes mellitus. In mice, these mutations cause insulin secretion to be lost initially and, as the disease progresses, beta cell mass and insulin content also disappear. We investigated whether defects in calcium signalling alone are sufficient to explain short-term and long-term islet dysfunction.

Methods We examined the metabolic, electrical and insulin secretion response in islets from mice that become diabetic after induction of ATP-insensitive Kir6.2 expression. To separate direct effects of K_{ATP} overactivity on beta cell function from indirect effects of prolonged hyperglycaemia, normal glycaemia was maintained by protective exogenous islet transplantation.

Results In endogenous islets from protected animals, glucose-dependent elevations of intracellular free-

calcium activity ($[\text{Ca}^{2+}]_i$) were severely blunted. Insulin content of these islets was normal, and sulfonylureas and KCl stimulated increased $[\text{Ca}^{2+}]_i$. In the absence of transplant protection, $[\text{Ca}^{2+}]_i$ responses were similar, but glucose metabolism and redox state were dramatically altered; sulfonylurea- and KCl-stimulated insulin secretion was also lost, because of systemic effects induced by long-term hyperglycaemia and/or hypoinsulinaemia. In both cases, $[\text{Ca}^{2+}]_i$ dynamics were synchronous across the islet. After reduction of gap-junction coupling, glucose-dependent $[\text{Ca}^{2+}]_i$ and insulin secretion was partially restored, indicating that excitability of weakly expressing cells is suppressed by cells expressing mutants, via gap-junctions.

Conclusions/interpretation The primary defect in K_{ATP} -induced neonatal diabetes mellitus is failure of glucose metabolism to elevate $[\text{Ca}^{2+}]_i$, which suppresses insulin secretion and mildly alters islet glucose metabolism. Loss of insulin content and mitochondrial dysfunction are secondary to the long-term hyperglycaemia and/or hypoinsulinaemia that result from the absence of glucose-dependent insulin secretion.

R. K. P. Benninger and M. S. Remedi contributed equally to this study.

Electronic supplementary material The online version of this article (doi:10.1007/s00125-010-2039-7) contains supplementary material, which is available to authorised users.

R. K. P. Benninger · W. S. Head · A. Ustione · D. W. Piston (✉)
Molecular Physiology and Biophysics, Vanderbilt University,
2215 Garland Avenue,
Nashville, TN 37232, USA
e-mail: dave.piston@vanderbilt.edu

M. S. Remedi · C. G. Nichols (✉)
Cell Biology and Physiology, Washington University,
660 S Euclid Avenue,
St Louis, MO 63110, USA
e-mail: cnichols@wustl.edu

Keywords Beta cell · Calcium · Gap-junctions · K_{ATP} channel · Neonatal diabetes mellitus · Transgenic mice

Abbreviations

DTG	Double transgenic
$[\text{Ca}^{2+}]_i$	Intracellular free-calcium activity
αGA	18- α -Glycyrrhetic acid
GFP	Green fluorescent protein
GSIS	Glucose-stimulated insulin secretion
K_{ATP}	ATP-sensitive potassium
TMRE	Tetramethyl-rhodamine ester

Introduction

Following glucose uptake into beta cells, increased intracellular [ATP]:[ADP] leads to inhibition of ATP-sensitive potassium (K_{ATP}) channels, which leads to insulin secretion via a cascade of membrane depolarisation, Ca^{2+} influx and increased intracellular free-calcium activity ($[Ca^{2+}]_i$) [1]. K_{ATP} channels in the beta cell are made up of inward rectifier $K(+)$ channel Kir6.2 and sulfonylurea receptor 1 subunits. Mutations in *KIR6.2* (also known as *KCNJ11*) or *SUR1* (also known as *ABCC8*) that reduce sensitivity to ATP-inhibition suppress glucose-stimulated insulin secretion (GSIS) [2]. In humans, such ‘gain-of-function’ mutations are the most common cause of neonatal diabetes mellitus [3]. The human disease was predicted by transgenic mice in which ATP-insensitive K_{ATP} channels were introduced into beta cells, leading to a profound neonatal diabetic phenotype [4], although neonatal death of these animals precluded detailed analysis of islet function. Mice expressing inducible gain-of-function Kir6.2 subunit mutations under Cre-recombinase control have now been generated [5, 6]. These animals show severe glucose intolerance within ~2 weeks of mutant- K_{ATP} channel expression and progress to a dramatic diabetic phenotype, with beta cell mass and insulin content both markedly declining with time [5]. Imposing glycaemic control via exogenous islet transplantation prior to transgene-induction avoids systemic diabetes and preserves endogenous islet beta cell mass and insulin content [5].

To gain further insight into the cellular mechanisms underlying neonatal diabetes mellitus, we examined glucose-dependent metabolic and $[Ca^{2+}]_i$ signalling as well as insulin secretion in islets from these animals. As K_{ATP} channels are the main regulator of islet electrical activity, we asked whether defects in Ca^{2+} signalling alone are sufficient to explain the altered islet function in neonatal diabetes mellitus. By imposing glycaemic control to protect endogenous islets from systemic diabetes, we examined the direct effects of the ATP-insensitive K_{ATP} channels on islet function and were able to separate these from the additional effects of systemic hyperglycaemia and hypoinsulinaemia on unprotected islets.

This mouse model also allowed us to test a previously proposed model of electrical coupling in the islet [7]; where less excitable cells suppress activity in more excitable cells via gap-junctions. Previous studies have been limited to the coupling of a loss-of-function (inhibition) in the K_{ATP} channel. Here we tested the role of gap-junction coupling in coordinating K_{ATP} gain-of-function across the islet and determined how this coupling impacts glucose-dependent $[Ca^{2+}]_i$ and insulin secretion responses.

Methods

Mouse model of K_{ATP} -induced neonatal diabetes mellitus All experiments were performed in compliance with the relevant laws and institutional guidelines, and were approved by the Washington University Animal Studies Committee. The generation of mice expressing *Rosa26-Kir6.2*[K185Q, Δ N30] mutant-transgene with green fluorescent protein (GFP) is described in detail elsewhere [5]. These mice were crossed with mice expressing *Pdx1*^{PB}-CreER [8] to generate pancreatic beta cell-specific double transgenic (DTG) mice. Littermate wild-type and single transgenic mice which have normal blood glucose levels and insulin secretion were used as controls [5]. At 8 weeks of age, control and DTG mice received five consecutive daily doses of tamoxifen (50 mg/g body weight, experimental days 0–4). DTG protected mice received a transplant of islets removed from wild-type mice. The transplant was placed under the kidney capsule 2 days prior to the initial tamoxifen injection, following described procedures [5, 9]. Blood glucose measurements were taken daily using a glucometer (Elite XL; Bayer, Leverkusen, Germany). Mice were killed at experimental days 24 to 28 for islet isolation.

Islet isolation and dispersal Islets were isolated by collagenase digestion as described in [10, 11] and maintained in islet medium (RPMI medium containing 10% fetal bovine serum (vol./vol.), 11 mmol/l glucose, 100 U/ml penicillin, 100 μ g/ml streptomycin) at 37°C under humidified 5% CO_2 for 24 to 48 h before imaging. To obtain dispersed beta cells, islets were washed in Ca^{2+} -free HBSS, then incubated at 37°C with trypsin/EDTA (both 0.01%, wt/vol.) for 5 min. Trypsin-treated islets were then dispersed by gently re-suspending in islet medium. Dispersed beta cells were plated on glass coverslips in multi-well plates and maintained for 24 to 48 h at 37°C and 5% CO_2 .

Insulin secretion assays Following overnight incubation in low glucose (5.6 mmol/l) CMRL-1066 medium, islets (ten per well) or dispersed cells (from ten islets per well) were pre-incubated for 30 min at 37°C in glucose-free CMRL-1066 plus 3 mmol/l glucose, then incubated for 60 min at 37°C in CMRL-1066 plus different glucose concentrations, 1 μ mol/l glibenclamide and 30 mmol/l KCl as indicated. When 18- α -glycyrrhetic acid (α GA) treatment was performed, islets were pre-incubated for 30 min with 10 or 50 μ mol/l α GA, prior to incubation with 10 or 50 μ mol/l α GA plus different glucose concentrations. The medium was then removed and assayed for insulin release. Islets were disrupted using ethanol-HCl extraction and sonicated on ice prior to estimation of insulin content.

Insulin secretion and content were measured in triplicates using rat insulin radioimmunoassay according to manufacturer's procedure (Linco, St Charles, MO, USA).

Widefield, confocal and two-photon microscopy To measure cellular $[Ca^{2+}]_i$ response and dynamics, isolated islets or dispersed beta cells were stained at room temperature for 1 to 3 h with 4 $\mu\text{mol/l}$ FuraRed-AM and/or 4 $\mu\text{mol/l}$ Fluo4-AM (Invitrogen, Carlsbad, CA, USA) in imaging medium (125 mmol/l NaCl, 5.7 mmol/l KCl, 2.5 mmol/l $CaCl_2$, 1.2 mmol/l $MgCl_2$, 10 mmol/l HEPES, 2 mmol/l glucose, 0.1% BSA (wt/vol.), pH 7.4). Intact islets were imaged in a polydimethylsiloxane microfluidic device [7], facilitating stable imaging and rapid reagent change. Dispersed beta cells were imaged in labtex dishes (Nunc, Roskilde, Denmark). Islets or beta cells were imaged in a humidified chamber maintained at 37°C using a slit-scanning microscope (LSM5Live, Zeiss, Jena, Germany) with a $\times 20$ 0.8NA Fluar objective. Images were acquired for 150 or 300 s at 10 min after glucose stimulation, 15 min after application of gap-junction inhibitor or immediately after sulfonylurea or KCl application. Fluo4- or GFP-fluorescence was detected using a 488 nm diode laser for excitation and a 495 to 555 nm band-pass filter for emission. FuraRed fluorescence was detected using the same diode laser and a 650 nm long-pass filter for emission. There was no detectable cross-talk between FuraRed and Fluo4/GFP channels. Background fluorescence was measured from unstained islets.

To measure absolute $[Ca^{2+}]_i$ levels, islets were stained for 30 min with 2 $\mu\text{mol/l}$ Fura2-AM and imaged at 37°C in a microfluidic device on a widefield microscope (TE-300; Nikon, Tokyo, Japan) with a 20 \times 0.45NA Fluar objective. Images were acquired 10 min after glucose stimulation. Islets were sequentially excited at 340 and 380 nm (± 10 nm band-pass filter), and fluorescence detected with a 470 to 550 nm band-pass filter. Background fluorescence was measured from unstained islets.

To measure NAD(P)H, islets were imaged at 37°C in a microfluidic device on an LSM710 microscope (Zeiss) with a $\times 40$ 1.2NA apochromatic water-immersion objective. NAD(P)H autofluorescence was detected using a 710 nm mode-locked Ti:sapphire laser oscillator (Coherent, Santa Clara, CA, USA) for two-photon excitation, and custom 380 to 500 nm band-pass filter (Chroma, Rockingham, VT, USA) and non-descanned detector for emission. GFP fluorescence was detected using a 488 nm Ar⁺ laser line for excitation and a 505 nm long-pass filter for emission. Z-stacks of six images were acquired at 2 μm spacing. No GFP fluorescence was detected in the NAD(P)H channel. All microscope and laser settings were kept constant between measurements.

To assess changes in mitochondrial membrane potential, islets were stained for 30 min with 50 nmol/l tetramethylrhodamine ester (TMRE), then imaged at 37°C in a microfluidic device on a LSM710 microscope with a $\times 40$ 1.2NA apochromatic water-immersion objective. Images were acquired 20 min after glucose stimulation. TMRE fluorescence was detected using a 561 nm diode-pumped solid-state laser for excitation and a 580 to 680 nm band-pass filter for emission. Z-stacks of six images were acquired at 2 μm spacing.

Data analysis Image analyses were performed in Matlab (Mathworks, Natick, MA, USA) and Image Examiner (Zeiss). To calculate fold changes in Fluo4/FuraRed ratio, Fluo4 and FuraRed fluorescence intensities were averaged across each islet and background subtracted. Fluo4/FuraRed intensity ratio was taken and averaged over the measurement time (150 s). For each islet, the mean Fluo4/FuraRed ratio was normalised to the ratio measured at 2 mmol/l glucose. For Fura2 measurements, 340 and 380 nm intensities were background-subtracted and averaged across each islet. Mean $[Ca^{2+}]_i$ levels were calibrated from background-subtracted 340:380 nm intensity ratio using a kit (Fura2 Calcium Calibration Kit; Invitrogen)

NAD(P)H and TMRE fluorescence were averaged across each islet and each z-position. To calculate NAD(P)H fluorescence in GFP-positive cells, a GFP threshold intensity was calculated from the mean autofluorescence level in the GFP channel from GFP-negative control islets. This threshold value excludes >99% of GFP-negative cells as measured in control islets. For GFP-positive and GFP-negative cells, NAD(P)H fluorescence was averaged over all pixels showing a GFP intensity greater or less than the threshold GFP value respectively.

To estimate the proportion of the islet showing dynamic changes in $[Ca^{2+}]_i$, Fluo4 or FuraRed images were smoothed with a 3 \times 3 filter and the standard deviation of pixel intensity calculated over the acquisition time course. An active area was defined as having a pixel intensity variance >2 SD above silent pixels calculated at 2 mmol/l glucose. To calculate $[Ca^{2+}]_i$ dynamics in GFP-positive cells, $[Ca^{2+}]_i$ was determined in cells showing a GFP fluorescence greater than that measured in control islets as above.

Synchronisation of $[Ca^{2+}]_i$ dynamics was determined as described [12] and assessed in cells that showed significant dynamic changes in $[Ca^{2+}]_i$ (see above). Briefly, the Fluo4 time course in each pixel was cross-correlated with a reference Fluo4 time course averaged over the islet. The maximum cross-correlation value was then taken for each pixel. Areas of the islet showing a maximum cross-

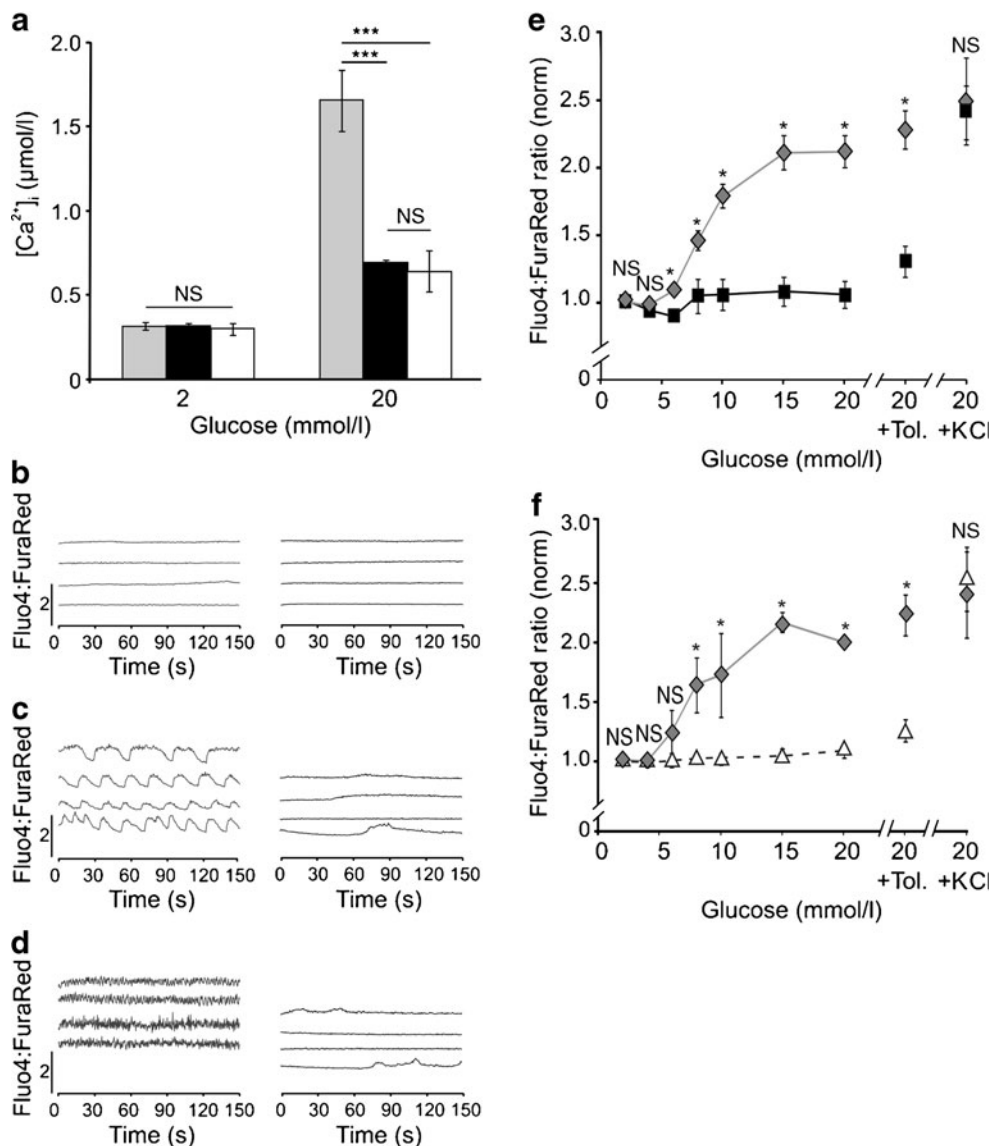


Fig. 1 Glucose-stimulated $[Ca^{2+}]_i$ activity in islets from DTG protected and DTG diabetic mice. **a** Mean $[Ca^{2+}]_i$ concentration in islets measured using Fura2 fluorescence. Islets were removed from control (grey bars), DTG protected (black bars) and DTG diabetic (white bars) mice, stimulated with 2 and 20 mmol/l glucose. *** $p < 0.001$ by the unpaired Student's t test. A significant increase in Ca^{2+} was observed at 20 mmol/l compared with 2 mmol/l glucose for DTG protected ($p < 0.01$) and DTG diabetic ($p < 0.05$). **b** Temporal progression of the Fluo-4/FuraRed ratio, averaged over single endogenous islets that were harvested from four different control mice (left) and from four different DTG protected mice (right), following 2 mmol/l glucose, **(c)** 10 mmol/l glucose and **(d)** 20 mmol/l glucose stimulation. Time courses are offset with respect to each

other for clarity, scale bar (y-axis) indicates twofold change in Fluo4/FuraRed. **e** Time-averaged Fluo4:FuraRed ratio in control islets (grey diamonds) and DTG protected islets (black squares), as a function of glucose concentration, glucose (20 mmol/l) plus sulfonylurea treatment (100 μ mol/l tolbutamide [Tol]) or glucose (20 mmol/l) plus KCl treatment (30 mmol/l). Data averaged over $n = 4$ mice, $n = 3$ –6 islets per mouse. **f** Time-averaged Fluo4:FuraRed ratio as above **(e)** for control islets (grey diamonds) and DTG diabetic islets (white triangles). Data averaged over $n = 4$ mice, $n = 3$ –4 islets per mouse. All Fluo4/FuraRed ratios were normalised (norm) to the ratio measured at 2 mmol/l glucose. * $p < 0.05$ and NS $p > 0.05$ for each experimental condition comparing control islets and DTG protected or DTG diabetic islets (unpaired Student's t test)

correlation > 0.5 represented areas that are synchronised. This synchronised area was expressed as a percentage of the total islet area that showed significant dynamic changes in $[Ca^{2+}]_i$.

Statistics Data are presented as mean \pm SEM. Unpaired or paired Student's t test was used to assess significance between control and DTG mouse groups. When more than two groups were tested, we assessed significance within

each condition tested using ANOVA and Duncan's post hoc test.

Results

Animal glucose and insulin levels To examine the cellular signalling events that underlie neonatal diabetes mellitus, islets were isolated from *Rosa26-Kir6.2*[K185Q,ΔN30]; *Pdx1^{fl/fl}-CreER* DTG mice, under two conditions: (1) DTG animals that underwent exogenous wild-type islet transplant prior to transgene induction (DTG protected); and (2) DTG animals that were not treated with islet transplant (DTG diabetic). DTG protected animals maintain normal blood glucose levels, while DTG diabetic animals experience a rise in blood glucose to 29.9 to 33.3 mmol/l (520 to 600 mg/dl) after about 3 weeks (Electronic supplementary material [ESM] Fig. 1). These glucose levels, as well as

islet insulin content (ESM Fig. 2) and insulin secretion (ESM Fig. 3) are consistent with previously published results [5, 6].

Ca²⁺ signalling in islets of DTG protected and DTG diabetic mice We first asked whether altered islet Ca²⁺ signalling can explain the altered insulin secretion in these mice. Islets from DTG protected and DTG diabetic mice showed similar [Ca²⁺]_i levels to control islets at low (2 mmol/l) glucose, but significant reduction in [Ca²⁺]_i levels at elevated (20 mmol/l) glucose (Fig. 1a). DTG protected and DTG diabetic islets still showed a small, but significant [Ca²⁺]_i elevation at 20 mmol/l glucose compared with 2 mmol/l glucose (Fig. 1a). Control islets exhibited no [Ca²⁺]_i dynamics at 2 mmol/l glucose, coordinated oscillations in [Ca²⁺]_i at 10 mmol/l glucose and continually elevated [Ca²⁺]_i at 20 mmol/l glucose (Fig. 1b–d). In contrast, DTG protected or DTG diabetic

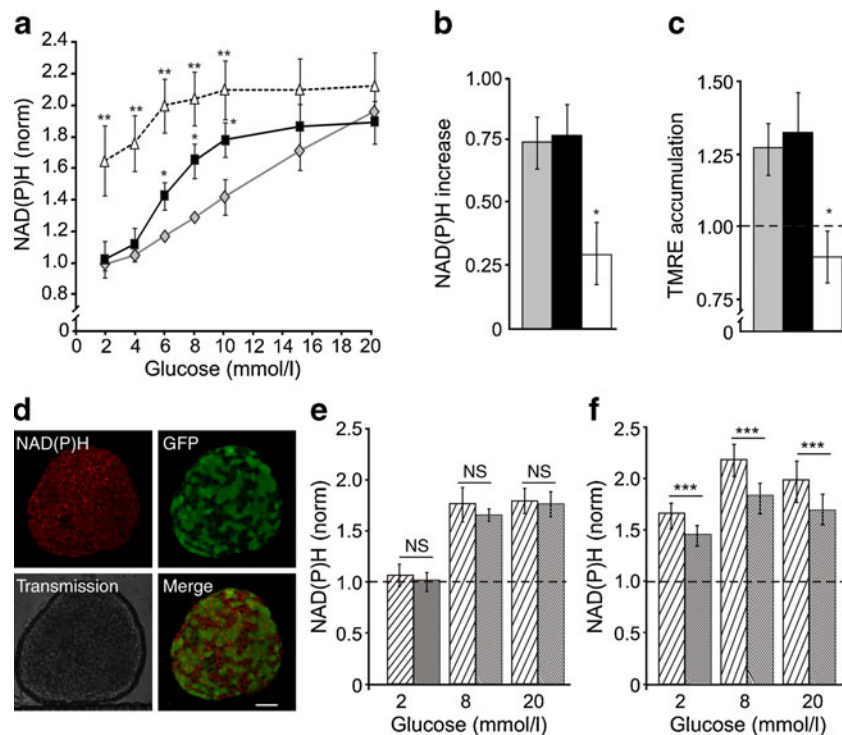


Fig. 2 Glucose metabolism in islets from DTG protected and DTG diabetic mice. **a** Glucose dose–response of NAD(P)H in islets from control (grey diamonds), DTG protected (black squares) and DTG diabetic (white triangles) mice, measured from normalised (norm) NAD(P)H fluorescence ($n=4$ mice, $n=4-6$ islets per mouse). **b** Change in NAD(P)H from 2 to 20 mmol/l glucose in islets of control (grey bars), DTG protected (black bars) and DTG diabetic (white bars) mice ($n=4$ mice, $n=4-6$ islets per mouse). **c** Mitochondrial TMRE accumulation in islets at 20 mmol/l glucose, normalised to TMRE fluorescence at 2 mmol/l, as represented above (**b**); $n=3$ mice, $n=4-7$ islets per mouse; $*p<0.05$ and $**p<0.01$ for each experimental condition (**a–c**) comparing control islets and DTG protected or DTG diabetic islets (unpaired Student's *t* test). **d** Pseudo-colour image of NAD(P)H fluorescence (red), GFP fluorescence (green) and transmission

(grey) in an islet from a DTG protected mouse. Separate channels and merged GFP/NAD(P)H images are shown. Scale bar, 50 μm . **e** Mean NAD(P)H fluorescence signal at glucose as indicated in islets from DTG protected mice. NAD(P)H fluorescence was measured in cells with high GFP fluorescence (GFP-positive; hatched bars) and low GFP fluorescence (GFP-negative; shaded bars); $n=7$ mice, $n=4-7$ islets per mouse. All data normalised (norm) to the mean NAD(P)H level in control islets at 2 mmol/l glucose (dotted grey line). **f** Mean NAD(P)H fluorescence signal as above (**e**) in islets from DTG diabetic mice; $n=5$ mice, $n=4$ islets per mouse). Mean and SEM (**e, f**) were calculated from absolute NAD(P)H values averaged over each mouse studied. For difference in means $\pm 95\%$ CI (**e, f**), see ESM Fig. 4a, b, respectively. $***p<0.001$ and NS $p>0.05$ (paired Student's *t* test)

islets showed irregular increases in $[Ca^{2+}]_i$ at elevated 10 and 20 mmol/l glucose levels (Fig. 1b–d). The mean glucose-dependent $[Ca^{2+}]_i$ response in DTG protected and DTG diabetic islets was severely blunted compared with control islets at all glucose levels >6 mmol/l (Fig. 1e, f). Tolbutamide and KCl at high glucose increased mean $[Ca^{2+}]_i$ to a similar extent in DTG protected and DTG diabetic islets, with the KCl response being similar to that of control islets in both cases. Thus, altered Ca^{2+} signalling is likely to underlie the altered insulin secretion in DTG protected islets (ESM Fig. 3), with no further impact on $[Ca^{2+}]_i$ during the initial development of hyperglycaemia and hypoinsulinaemia in DTG diabetic islets.

Glucose metabolism in islets of DTG protected and DTG diabetic mice We next examined the redox state in these islets to test whether the impact of mutant K_{ATP} channels is limited to Ca^{2+} signalling or whether these mutant channels also impact more proximal events in GSIS. Control and DTG protected islets showed similar NAD(P)H response to glucose, as assessed by two-photon microscopy [13], although NAD(P)H was more elevated in DTG protected islets at 6 to 10 mmol/l glucose (Fig. 2a).

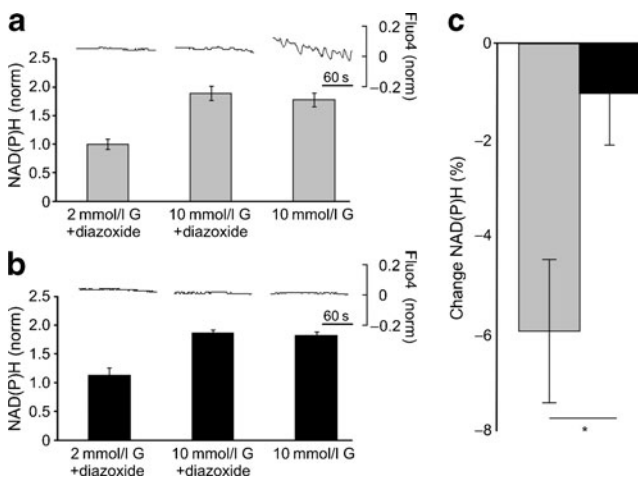


Fig. 3 Glucose metabolism in islets from DTG protected mice upon modulation of $[Ca^{2+}]_i$. **a** Normalised (norm) NAD(P)H and normalised Fluo4 time course in control islets upon stimulation with glucose (G) and diazoxide treatment as indicated. NAD(P)H was measured first, then a Fluo4 fluorescence time course was measured before and after elevation of glucose from 2 to 10 mmol/l in the presence of 250 μ mol/l diazoxide. NAD(P)H and Fluo4 fluorescence time course were subsequently measured following wash-off of diazoxide. Time between measurements of NAD(P)H was 20 min. Values are mean \pm SEM. NAD(P)H signal and a representative time course of Fluo4 fluorescence are shown for each glucose and diazoxide treatment. Horizontal scale bar 60 s. **b** As above (**a**), but with DTG protected islets. **c** Mean per cent change in NAD(P)H at 10 mmol/l glucose compared with NAD(P)H at the same glucose concentration in the presence of 250 μ mol/l diazoxide in islets of control (grey bar) and DTG protected (black bar) mice. * p <0.05 (paired Student's t test)

In contrast, significantly elevated NAD(P)H levels were seen in DTG diabetic islets at 2 to 10 mmol/l glucose. DTG diabetic islets exhibited a higher level of NAD(P)H at 2 mmol/l glucose, and a lower NAD(P)H increase between 2 and 20 mmol/l glucose (Fig. 2b). Total cellular NAD(P)H/NAD(P) is dominated by mitochondrial NADH signal [14], so these differences in NAD(P)H are likely to reflect altered mitochondrial function. Consistent with this, DTG protected and control islets showed significant accumulation of the mitochondrial membrane potential dye TMRE at elevated glucose levels, indicating mitochondrial membrane depolarisation. However there was no significant glucose-dependent TMRE accumulation in DTG diabetic islets (Fig. 2c).

A significant fraction of cells in DTG islets ($55 \pm 3\%$ of cells, averaged over five mice, two to six islets per mouse) showed GFP fluorescence intensity above that of the autofluorescence measured in control islets (Fig. 2d). Wide variation in GFP levels between cells implies a wide variation in *Rosa26-Kir6.2*[K185Q, Δ N30] transgene expression between individual beta cells in the islet. We therefore measured NAD(P)H levels in individual cells in DTG islets and grouped them into cells with high or low levels of GFP. There were no significant differences between NAD(P)H levels in GFP-positive and GFP-negative cells at any glucose concentrations in DTG protected islets (Fig. 2e), although a significant elevation in NAD(P)H was seen in DTG diabetic islet cells with high levels of GFP (Fig. 2f, ESM Fig. 4). This indicates that secondary consequences of diabetes have a significant effect on cellular metabolism, particularly affecting the redox state and mitochondrial membrane potential. This appears to be more prominent in cells expressing the transgene at higher levels.

Coupling of $[Ca^{2+}]_i$ and glucose metabolism in DTG protected mice In DTG protected islets, small but significant elevations in NAD(P)H at 6 to 10 mmol/l glucose (Fig. 2a) partially correlated with reduced glucose-dependent $[Ca^{2+}]_i$ elevation (Fig. 1e). Mitochondrial Ca^{2+} uptake regulates mitochondrial function and ATP synthesis [15, 16]. To test whether reduced glucose-dependent $[Ca^{2+}]_i$ underlies the elevated redox state in DTG protected islets, we stimulated control and DTG protected islets with 10 mmol/l glucose in the presence of diazoxide to prevent elevation in $[Ca^{2+}]_i$ without direct modulation of NADH oxidation [17]. As expected, NAD(P)H was elevated in control islets (Fig. 3a) and DTG protected islets (Fig. 3b) following elevated glucose. Removal of diazoxide led to a recovery of elevated oscillatory $[Ca^{2+}]_i$ (Fig. 3a) and a small but significant reduction of NAD(P)H in control islets (Fig. 3c), but no change to either signal in DTG protected islets (Fig. 3c). The observed increase in NAD(P)H in DTG

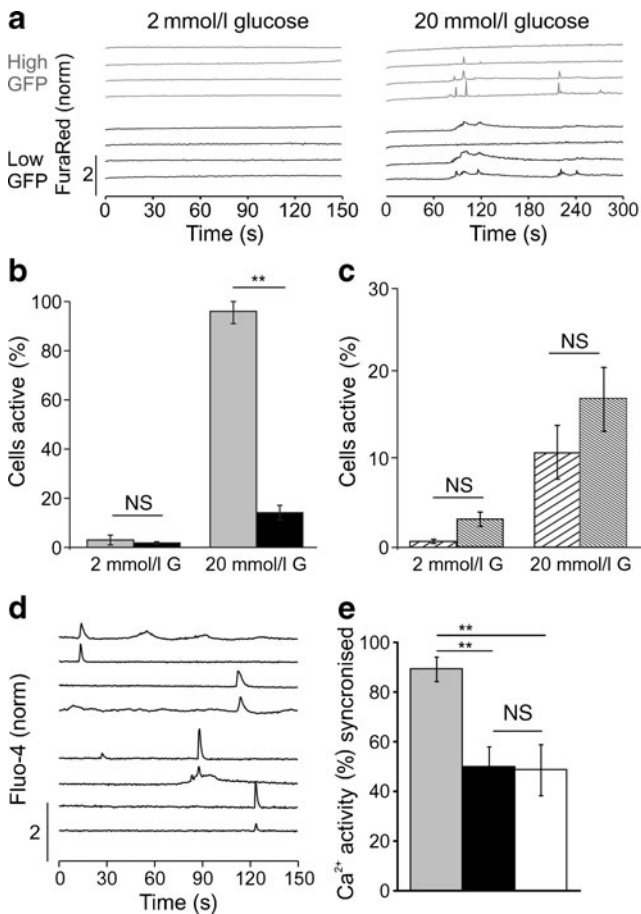


Fig. 4 $[Ca^{2+}]_i$ in individual cells of DTG protected islets. **a** Time course of normalised (norm.) FuraRed fluorescence from a single DTG protected islet in cells with GFP expression and at glucose concentrations as indicated. Scale bar represents twofold change in FuraRed. **b** Per cent of islet cells showing changes in $[Ca^{2+}]_i$ at 2 or 20 mmol/l glucose (G), as shown above (a), for islets from control mice (grey bars) and DTG protected mice (black bars). $**p < 0.01$ (unpaired Student's *t* test). **c** Per cent of DTG protected islet cells showing $[Ca^{2+}]_i$ bursting in cells with high GFP (hatched bars) and low GFP (shaded bars). Data (b, c) are average of $n = 4$ mice, $n = 3$ –5 islets per mouse. NS $p > 0.05$. **d** Time course of normalised Fluo4 fluorescence, illustrated by two sets of traces, in several cells from two representative DTG diabetic islets stimulated with 20 mmol/l glucose. Some synchronised $[Ca^{2+}]_i$ bursting can be seen by simultaneous changes in Fluo4 signal. Scale bar represents twofold change in Fluo-4. **e** Quantification of the synchronisation of $[Ca^{2+}]_i$ bursting in control islets (grey bars), DTG protected islets (black bars) and DTG diabetic islets (white bars), all at 10 mmol/l glucose stimulation. $**p < 0.01$ (unpaired Student's *t* test)

protected islets at 6 to 10 mmol/l glucose can, at least partly, be explained by the absence of a glucose-dependent $[Ca^{2+}]_i$ increase.

Cell–cell coupling of $[Ca^{2+}]_i$ in islets of DTG protected islets Since we observed cell-to-cell variation of transgene expression in DTG islets, we asked what impact this has on the cellular $[Ca^{2+}]_i$ response. We examined the correlation

between the presence of $[Ca^{2+}]_i$ oscillations and *Rosa26-Kir6.2*[K185Q,ΔN30] transgene expression in individual cells in DTG protected islets. At 20 mmol/l glucose, sub-regions of DTG protected islets showed occasional dynamic changes in $[Ca^{2+}]_i$ ($[Ca^{2+}]_i$ bursts) at irregular intervals, which were sometimes synchronised across the islet (Fig. 4a) and were detected in cells with high and low levels of GFP. In DTG protected islets at 20 mmol/l glucose only $14 \pm 5\%$ of the cells showed such bursting activity, compared with $>90\%$ of cells in control islets (Fig. 4b). No significant difference in the proportion of active cells was measured when comparing cells with high or low GFP (Fig. 4c), although the duration of a $[Ca^{2+}]_i$ burst was much reduced in cells with high GFP (3 ± 1 s) compared with cells with low GFP (30 ± 6 s). Similarly, occasional synchronous $[Ca^{2+}]_i$ bursts were measured in DTG diabetic islets (Fig. 4d). Synchronisation in DTG protected and DTG diabetic islets was reduced to a similar degree compared with control islets, such that only about 50% of $[Ca^{2+}]_i$ bursts were synchronised (Fig. 4e).

The synchronised $[Ca^{2+}]_i$ bursts in DTG protected islets suggests the presence of coupled electrical activity, despite the expression of overactive K_{ATP} channels. Previous studies have indicated that gap-junction coupling can suppress $[Ca^{2+}]_i$ elevations [7]. To test the role of gap-junction coupling in regulating the $[Ca^{2+}]_i$ response in islets with overactive K_{ATP} channels, we measured $[Ca^{2+}]_i$ in DTG protected islets at 20 mmol/l glucose following partial inhibition of gap-junctions by α GA [7]. All DTG protected islets showed an increase in the number of active cells at elevated glucose after partial gap-junction inhibition (Fig. 5a). No significant difference in the proportion of cells with synchronous $[Ca^{2+}]_i$ bursts was measured (not shown). KCl treatment further elevated $[Ca^{2+}]_i$ in most cells of the islet ($94 \pm 2\%$). Application of α GA at high glucose also led to elevated insulin secretion in DTG protected, but not in control islets (Fig. 5b).

Complete loss of cell–cell coupling can be achieved by dispersing islets into single cells (ESM Fig. 5). At low glucose, DTG protected cells showed no difference in $[Ca^{2+}]_i$ compared with control cells. At high glucose, $50 \pm 2\%$ of the DTG protected cells exhibited bursting (Fig. 5c), which was significantly higher than in intact DTG protected islets ($14 \pm 5\%$) (Fig. 4b), but lower than in control cells ($>90\%$). The $[Ca^{2+}]_i$ bursts at elevated glucose were restricted to GFP-negative cells (Fig. 5d), with GFP-positive beta cells remaining silent. Dispersed cells from DTG protected islets also showed a significant increase in insulin secretion at high glucose; although the fold change of insulin secretion from 1 to 23 mmol/l glucose (2.11 ± 0.37) was not significantly different from that measured in intact DTG protected islets (1.77 ± 0.48) (ESM Fig. 1) and was smaller than in control cells (Fig. 5e).

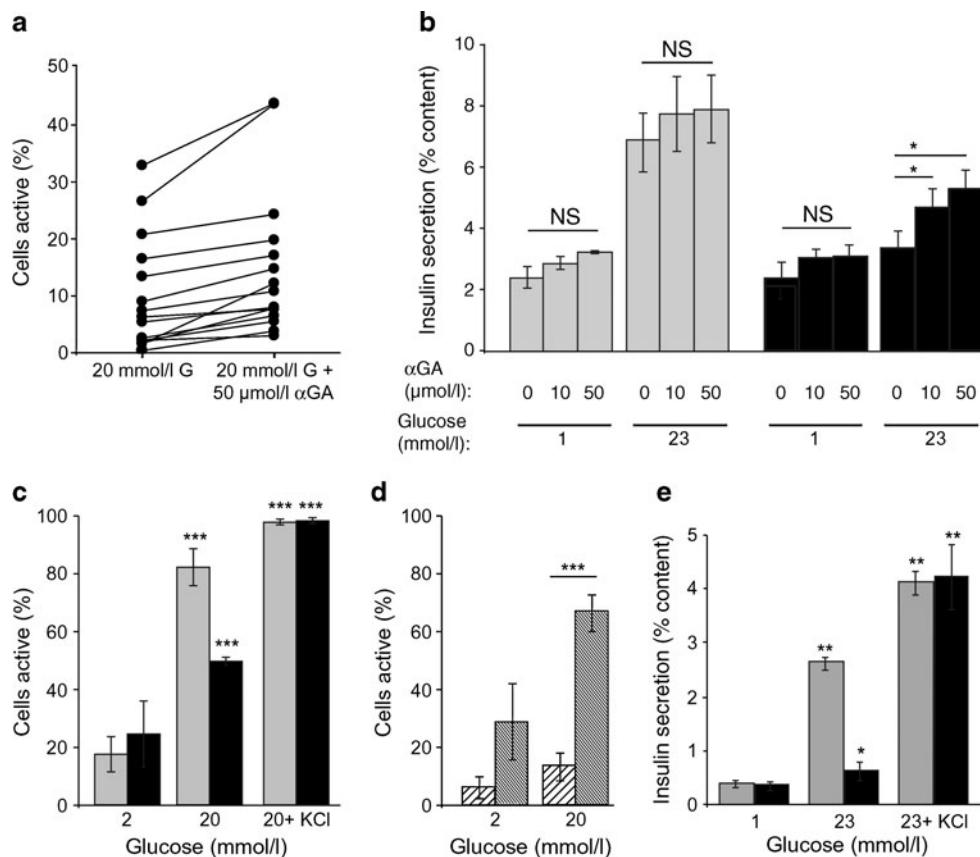


Fig. 5 Ca^{2+} activity and insulin secretion are increased in DTG protected islets upon reduction of gap-junction coupling. **a** Percentage of cells showing $[\text{Ca}^{2+}]_i$ bursting at 20 mmol/l glucose in 14 DTG protected islets before and after application of the gap-junction inhibitor αGA (50 $\mu\text{mol/l}$). An increase was seen in all 14 islets studied (isolated from four mice). **b** Insulin secretion from islets of control mice (grey bars) and DTG protected mice (black bars), stimulated with 1 or 23 mmol/l glucose and αGA (0, 10 or 50 $\mu\text{mol/l}$), as indicated. * $p < 0.05$ and NS $p > 0.05$ (unpaired Student's t test). **c** Per cent of isolated cells showing $[\text{Ca}^{2+}]_i$ bursting at glucose or glucose plus KCl (30 mmol/l) as indicated from islets of control mice (grey bars) and

DTG protected mice (black bars). * $p < 0.05$ for each experimental condition vs 2 mmol/l glucose within each group. **d** Percentage of isolated cells showing $[\text{Ca}^{2+}]_i$ bursting in cells with high GFP (hatched bars) and low GFP (shaded bars). Data (**c**, **d**) averaged over $n = 3$ mice; $n = 2\text{--}3$ cell preparations per mouse. *** $p < 0.001$ (unpaired Student's t test). **e** Insulin secretion, normalised to insulin content, in dispersed cells from islets of control (grey bars) or DTG protected (black bars) mice, stimulated with glucose as indicated or with glucose as indicated plus KCl (30 mmol/l). Data averaged over $n = 4$ mice, three cell preparations per mouse. * $p < 0.05$ and ** $p < 0.01$ for each experimental condition vs 1 mmol/l glucose within each group

Discussion

In this study we sought to uncover the cellular mechanisms by which 'gain-of-function' K_{ATP} channel mutations underlie neonatal diabetes mellitus. We hypothesised that the overactivity of these K_{ATP} channels causes a loss of Ca^{2+} signalling, leading directly to defective GSIS. Additionally, we asked whether this loss of Ca^{2+} signalling has an additional impact on beta cell function. Previous studies have shown that K_{ATP} overactivity causes loss of GSIS [5, 6] with resultant hyperglycaemia and/or hypoinsulinaemia, leading to further loss of beta cell mass and insulin content [5]. The use of inducible *Rosa26-Kir6.2* [K185Q, Δ N30] mice along with islet transplantation to maintain normoglycaemia allowed us to separate the primary effects of K_{ATP} overactivity on beta cell function

and provided a rigorous test of how the secondary consequences of neonatal diabetes mellitus impact on islet function and insulin secretion. We therefore further asked how beta cell function is subsequently altered in this model of neonatal diabetes mellitus as a consequence of systemic hyperglycaemia and hypoinsulinaemia.

Altered Ca^{2+} signalling underlies altered insulin secretion in neonatal diabetes mellitus islets The primary effect of the *Kir6.2* gain-of-function mutation was to dramatically suppress glucose-dependent $[\text{Ca}^{2+}]_i$ (Fig. 1) and thus reduce glucose-dependent insulin secretion. In addition to direct triggering of insulin secretion, elevated $[\text{Ca}^{2+}]_i$ leads to Ca^{2+} uptake into the mitochondria, which can stimulate oxidative phosphorylation and ATP synthesis via activation of several dehydrogenases [15, 16]. In DTG protected islets,

we measured a small increase in NAD(P)H at intermediate glucose levels between 6 and 10 mmol/l (Fig. 2), which was in part dependent on the absence of glucose-stimulated $[Ca^{2+}]_i$ elevation (Fig. 3). These results are consistent with previous studies suggesting that a Ca^{2+} -dependent activation of the respiratory chain [18] occurs in normal islets at glucose levels of around 10 mmol/l [19], which counteracts Ca^{2+} -dependent elevation of NAD(P)H as a result of elevated oxidative phosphorylation. Therefore the elevated NAD(P)H levels we measured in DTG protected islets could have resulted from a lack of Ca^{2+} -dependent NADH oxidation by the respiratory chain. According to previous observations [19], this would further predict a decrease in ATP synthesis. In this way, K_{ATP} overactivity and consequent lack of Ca^{2+} signalling would play a direct role in glucose metabolism and ATP synthesis. This may also alter other mitochondrial signalling mechanisms and affect insulin secretion, since mitochondrial GTP synthesis is an important component of GSIS [20]. However, as discussed below, other changes in glucose metabolism and mitochondrial function were found after systemic diabetes, so these processes may also have been important contributors to secondary changes in islet function.

In DTG protected islets sulfonylureas triggered limited $[Ca^{2+}]_i$ and insulin secretory responses at levels lower than those seen in control islets. This is consistent with the reductive effect of *Kir6.2* gain-of-function mutations on sulfonylurea sensitivity of K_{ATP} channel activity [21, 22]. Given the low level of sulfonylurea-stimulated $[Ca^{2+}]_i$, sulfonylurea-stimulated insulin secretion was greater than expected, which may be attributable to the different drugs applied, but also may have originated from sulfonylurea-activated protein kinase C (PKC) or exchange protein directly activated by cAMP 2 (EPAC2) [23, 24]. Since the levels of KCl-stimulated $[Ca^{2+}]_i$ and insulin secretion in DTG protected islets were similar to those in control islets, a broader effect on Ca^{2+} influx or exocytotic capacity resulting from expression of overactive K_{ATP} channels does not seem to exist.

Secondary diabetic consequences are independent of $[Ca^{2+}]_i$ Glucose-dependent $[Ca^{2+}]_i$ was similarly suppressed in DTG protected and DTG diabetic islets, and sulfonylurea- and KCl-stimulated $[Ca^{2+}]_i$ was essentially the same in both (Fig. 1). However, there was a clear difference in their metabolic (Fig. 2) and insulin secretory (ESM Fig. 1) responses. The chronic hyperglycaemia in DTG diabetic mice could alter beta cell glucose sensing [25] or glucose metabolism [26]. Elevated NAD(P)H at low glucose indicates an elevated redox state in islets from diabetic animals. The absence of glucose-dependent NAD(P)H and TMRE accumulation further indicates a lack of elevated glucose metabolism and mitochondrial membrane depolar-

isation at elevated glucose. Thus, the defective mitochondrial function we measured in DTG diabetic islets could have been due to absence of electron transport and a marked decrease in NADH oxidation, which would suggest decreased ATP synthesis. Total nicotinamide adenine dinucleotide levels ($NAD^+ + NADP^+ + NADH + NADPH$) are typically constant [27, 28], although this has not been verified in islets chronically exposed to diabetic conditions. Therefore we cannot rule out the possibility that total nicotinamide adenine dinucleotide levels became elevated in our DTG diabetic islets. Absence of any elevation in $[Ca^{2+}]_i$ at 2 mmol/l glucose (from ATP-dependent K_{ATP} channel inhibition) strongly argues against the possibility that NAD^+ reduction is constitutively high from citric acid cycle metabolism and ATP synthesis. Interestingly, similar mitochondrial defects have also been observed in the absence of beta cell insulin signalling [29], suggesting that the hypoinsulinaemia in DTG diabetic mice may also have contributed to islet dysfunction.

Cell–cell coupling in protected and diabetic K_{ATP} gain-of-function islets The varied expression levels of the *Rosa26-Kir6.2*[K185Q, Δ N30] transgene between cells (Fig. 2) suggests that the intrinsic excitability among beta cells of DTG islets is also varied. However, we observed substantial synchronisation of $[Ca^{2+}]_i$ dynamics in DTG protected and DTG diabetic islets (Fig. 4), regardless of the levels of transgene expression. This indicates that a coordination of K_{ATP} overactivity occurs throughout the islets, independently of individual cellular *Rosa26-Kir6.2*[K185Q, Δ N30] transgene expression. Therefore, despite incomplete penetrance of the mutant transgene, normal levels of electrical coupling and coordination within the islet can ensure that the effect of the transgene is felt throughout, accurately reflecting the expected condition in neonatal diabetes mellitus.

Previous studies have shown that normal beta cells can suppress excitability of neighbouring hyperexcitable beta cells via gap-junction channels [7, 30]. Our observations extend this finding by showing that underexcitable cells with high levels of *Kir6.2* gain-of-function transgene expression can suppress excitability of cells with low transgene expression. This suppression occurs via gap-junction channels: a reduction in gap-junction coupling by chemical inhibition or dispersion into isolated cells leads to elevation in the number of cells exhibiting $[Ca^{2+}]_i$ bursting and elevated glucose-dependent insulin secretion from DTG protected islets, but not from control islets (Fig. 5). Gap-junctional coupling allows suppression of normally excitable cells by inexcitable cells and therefore can have a significant effect on the insulin secretion response.

Finally, we noted a significant synchronisation of Ca^{2+} activity between cells in DTG diabetic islets, in contrast to

previous reports in a similar mouse model of K_{ATP} -induced neonatal diabetes mellitus [6]. The difference might be explained by longer exposure of the islets to systemic hyperglycaemia in the earlier study (>5 weeks compared with ~3 weeks in our study). This extended pathological exposure would lead to more advanced secondary complications including loss of beta cell mass [5], and could be accompanied by a downregulation of gap-junctions [31] and reduced coupling of $[Ca^{2+}]_i$.

Conclusion

We found that ATP-insensitive K_{ATP} channels inhibited glucose-stimulated $[Ca^{2+}]_i$, underlying defective insulin secretion. Loss of elevated $[Ca^{2+}]_i$ further affected glucose metabolism and mitochondrial function, but had no effect on distal steps involving voltage-dependent Ca^{2+} influx and exocytotic capability. As a result of prolonged systemic hyperglycaemia in DTG diabetic animals, islet glucose metabolism and mitochondrial function were severely disrupted and insulin content was lost, but Ca^{2+} signalling was not further affected. Electrical coupling overcomes cell–cell variability of transgene expression and coordinates K_{ATP} overactivity across the islet. This coordination allows this murine model to accurately reproduce the effects of neonatal diabetes mellitus despite variable expression of the transgene.

Acknowledgements This study was primarily supported by NIH grants K99-DK85145 (to R. K. P. Bennisger), R01-DK69445 (to C. G. Nichols) and R01-DK53434, P20-GM72048 (to D. W. Piston), as well as by the Department of Defence Medical Free-Electron Laser Program. Experiments on the LSM5Live were performed in part through the use of VUMC Cell Imaging Shared Resource.

Duality of interest The authors declare that there is no duality of interest associated with this manuscript.

References

- Nichols CG (2006) K_{ATP} channels as molecular sensors of cellular metabolism. *Nature* 440:470–476
- Hattersley AT, Ashcroft FM (2005) Activating mutations in Kir6.2 and neonatal diabetes—new clinical syndromes, new scientific insights, and new therapy. *Diabetes* 54:2503–2513
- Gloyn AL, Pearson ER, Antcliff JF et al (2004) Activating mutations in the gene encoding the ATP-sensitive potassium-channel subunit Kir6.2 and permanent neonatal diabetes. *N Engl J Med* 350:1838–1849
- Koster JC, Marshall BA, Ensor N, Corbett JA, Nichols CG (2000) Targeted overactivity of beta cell K_{ATP} channels induces profound neonatal diabetes. *Cell* 100:645–654
- Remedi MS, Kurata HT, Scott A et al (2009) Secondary consequences of beta cell inexcitability: identification and prevention in a murine model of K_{ATP} -induced neonatal diabetes mellitus. *Cell Metab* 9:140–151
- Girard CA, Wunderlich FT, Shimomura K et al (2009) Expression of an activating mutation in the gene encoding the K_{ATP} channel subunit Kir6.2 in mouse pancreatic beta cells recapitulates neonatal diabetes. *J Clin Invest* 119:80–90
- Rocheleau JV, Remedi MS, Granada B et al (2006) Critical role of gap junction coupled K_{ATP} channel activity for regulated insulin secretion. *PLoS Biol* 4:221–227
- Zhang HJ, Fujitani Y, Wright CVE, Gannon M (2005) Efficient recombination in pancreatic islets by a tamoxifen-inducible Cre-recombinase. *Genesis* 42:210–217
- Montana E, Bonnerweir S, Weir GC (1993) Beta-cell mass and growth after syngeneic islet cell transplantation in normal and streptozocin diabetic c57bl/6 mice. *J Clin Invest* 91:780–787
- Scharp DW, Kemp CB, Knight MJ, Ballinge WF, Lacy PE (1973) Use of ficoll in preparation of viable islets of Langerhans from rat pancreas. *Transplantation* 16:686–689
- Koster JC, Remedi MS, Flagg TP et al (2002) Hyperinsulinism induced by targeted suppression of beta cell K_{ATP} channels. *Proc Natl Acad Sci USA* 99:16992–16997
- Benninger RKP, Zhang M, Head WS, Satin LS, Piston DW (2008) Gap junction coupling and calcium waves in the pancreatic islet. *Biophys J* 95:5048–5061
- Bennett BD, Jetton TL, Ying GT, Magnuson MA, Piston DW (1996) Quantitative subcellular imaging of glucose metabolism within intact pancreatic islets. *J Biol Chem* 271:3647–3651
- Patterson GH, Knobel SM, Arkhammar P, Thastrup O, Piston DW (2000) Separation of the glucose-stimulated cytoplasmic mitochondrial NAD(P)H responses in pancreatic islet beta cells. *Proc Natl Acad Sci USA* 97:5203–5207
- McCormack JG, Halestrap AP, Denton RM (1990) Role of calcium-ions in regulation of mammalian intramitochondrial metabolism. *Physiol Rev* 70:391–425
- Wiederkehr A, Wollheim CB (2006) Minireview: implication of mitochondria in insulin secretion and action. *Endocrinology* 147:2643–2649
- Hanley PJ, Mickel M, Loffler M, Brandt U, Daut J (2002) K_{ATP} channel-independent targets of diazoxide and 5-hydroxydecanoate in the heart. *J Physiol Lond* 542:735–741
- Robb-Gaspers LD, Burnett P, Rutter GA, Denton RM, Rizzuto R, Thomas AP (1998) Integrating cytosolic calcium signals into mitochondrial metabolic responses. *EMBO J* 17:4987–5000
- Luciani DS, Misler S, Polonsky KS (2006) Ca^{2+} controls slow NAD(P)H oscillations in glucose-stimulated mouse pancreatic islets. *J Physiol Lond* 572:379–392
- Kibbey RG, Pongratz RL, Romanelli AJ, Wollheim CB, Cline GW, Shulman GI (2007) Mitochondrial GTP regulates glucose-stimulated insulin secretion. *Cell Metab* 5:253–264
- Koster JC, Remedi MS, Dao C, Nichols CG (2005) ATP and sulfonylurea sensitivity of mutant ATP-sensitive K^+ channels in neonatal diabetes—implications for pharmacogenomic therapy. *Diabetes* 54:2645–2654
- Proks P, Antcliff JF, Lippiat J, Gloyn AL, Hattersley AT, Ashcroft FM (2004) Molecular basis of Kir6.2 mutations associated with neonatal diabetes or neonatal diabetes plus neurological features. *Proc Natl Acad Sci USA* 101:17539–17544
- Eliasson L, Renstrom E, Ammala C et al (1996) PKC-dependent stimulation of exocytosis by sulfonylureas in pancreatic beta cells. *Science* 271:813–815
- Zhang CL, Katoh M, Shibasaki T et al (2009) The cAMP sensor Epac2 is a direct target of antidiabetic sulfonylurea drugs. *Science* 325:607–610

25. Jonas JC, Sharma A, Hasenkamp W et al (1999) Chronic hyperglycemia triggers loss of pancreatic beta cell differentiation in an animal model of diabetes. *J Biol Chem* 274:14112–14121
26. Roche E, Farfari S, Witters LA et al (1998) Long-term exposure of beta-INS cells to high glucose concentrations increases anaplerosis, lipogenesis, and lipogenic gene expression. *Diabetes* 47:1086–1094
27. Masters BR, Ghosh AK, Wilson J, Matschinsky FM (1989) Pyridine-nucleotides and phosphorylation potential of rabbit corneal epithelium and endothelium. *Investig Ophthalmol Vis Sci* 30:861–868
28. Matschinsky FM, Ghosh AK, Meglasson MD, Prentki M, June V, Vonallman D (1986) Metabolic concomitants in pure, pancreatic beta-cells during glucose-stimulated insulin-secretion. *J Biol Chem* 261:14057–14061
29. Liu SM, Okada T, Assmann A et al (2009) Insulin signaling regulates mitochondrial function in pancreatic beta-cells. *PLoS ONE* 4(11):e7983
30. Speier S, Gjinovci A, Charollais A, Meda P, Rupnik M (2007) Cx36-mediated coupling reduces beta-cell heterogeneity, confines the stimulating glucose concentration range, and affects insulin release kinetics. *Diabetes* 56:1078–1086
31. Allagnat F, Martin D, Condorelli DF, Waeber G, Haefliger JA (2005) Glucose represses connexin36 in insulin-secreting cells. *J Cell Sci* 118:5335–5344